ISSN: 2692-5397
DOI: 10.33552/MCMS.2024.06.000636
Modern Concepts in Material Science
Iris Publishers
Research article

Tool Wear Influence on The Fatigue Life of Lathe Processed Specimens of 1.6310 Steel

Fabian Weber[1,2], Tina Eyrisch[3], Torsten Hielscher[4]*

[1]*Department of Materials Science and Materials Testing (WWHK), Institute QM[3], University of Applied Sciences Kaiserslautern, Germany*

[2]*Faculty of Natural Sciences and Technology, Saarland University, Germany*

[3]*Institute QM[3], University of Applied Sciences Kaiserslautern, Germany*

[4]*Department of Mechanical Engineering (FHK), Institute QM[3], University of Applied Sciences Kaiserslautern, Germany*

***Corresponding author:** Torsten Hielscher, Department of Mechanical Engineering (FHK), Institute QM[3], University of Applied Sciences Kaiserslautern, Schoenstraße 11, 67659 Kaiserslautern, Germany.

Received Date: July 08, 2024

Published Date: July 23, 2024

Abstract

Machining processes result in numerous influencing factors on the fatigue behavior of manufactured specimens or components. In addition to various process parameters, such as feed rate, cutting speed and cutting depth, the wear condition of the cutting tools is a particularly important influencing factor. In the present work, the relationship between the wear condition of turning tools, represented by flank wear and cutting edge rounding, and the surface roughness of machined specimens is presented and their influence on fatigue behavior is investigated. Experiments were carried out on the ferritic-bainitic steel 1.6310 (20MnMoNi5-5), which is mainly used in spray lines in German nuclear power plants. The aim of the presented research is to attribute the scattering of fatigue life to the respective tool wear at given stress amplitudes.

Keywords: Turning; Tool Wear; Surface Roughness; Surface Integrity; Fatigue Life

Introduction

The fatigue behavior of metallic materials is characterized by a large number of influencing factors. In the High-Cycle-Fatigue (HCF)-regime in particular, fatigue is dominated by crack initiation from the surface, which is why parameters such as surface roughness and residual stresses are of great importance. Both influencing factors are essentially defined by the manufacturing process. Therefore, an in-depth understanding of the manufacturing influence is crucial for a reliable lifetime assessment. One of the most common manufacturing methods to machine materials is the turning process [1]. In addition to the selected machining parameters, in particular the wear condition of the tools has a direct effect on the surface integrity of the machined workpieces. The surface integrity in turn influences the fatigue behavior of components [2].

Investigations on the impact of machining parameters on tool wear and thus on the microgeometry of the cutting edge are the subject of numerous research projects in machining and especially in turning. For example, [1,3-6] present extensive results on the influence of cutting speed, feed and hardness of the machined material on tool wear for selected tempering steels.

It is generally assumed that there is a direct relationship between the wear behavior of cutting tools and their service life [7,8], and that progressive tool wear not only influences the dimensional accuracy of the machined components, but also in particular the surface roughness and the residual stress near the surface [9,10]. De Farias et al. [11] used artificially worn tool inserts in their work to create a data set to train a machine learning model for monitoring tool wear in machining processes.

The surface quality of machined components is primarily influenced by the macrogeometry of the cutting tool, the microgeometry of the cutting edge and the variation of the machining parameters. During the turning process, the geometry of the cutting tools is reproduced on the machined surface. Therefore, the feed rate is an important process parameter that influences the theoretical kinematic roughness [6,10]. In addition, feed rate and cutting speed have an impact on the surface integrity. Several studies show that the feed rate influences the formation of residual stresses [12,13], especially in fine machining [14]. In hard machining, on the other hand, the effect of the cutting speed on the formation of residual stresses predominates due to the greater thermoplastic deformation [15].

Numerous research papers also deal with the impact of the microgeometry of the tool's cutting edge on the induction of near-surface residual stresses. Liu, Takagi and Tsukuda [16] investigated the tool wear's influence on the residual stresses during hard turning of 100Cr6 (SAE 52100). Generally, progressive tool wear causes an increase in friction and process temperatures. Increasing passive forces were observed, particularly with larger cutting radii. With increasing tool wear, the residual tensile stresses on the workpiece surface and the penetration depth into the material increased. The latter increasingly led to residual compressive stresses. Fangyuan et al. [17] show a connection between increasing wear mark width and increasing residual tensile stresses during hard turning of 100Cr6. A link between the wear mark width (VB) of turning tools and the fatigue behavior is demonstrated by Gvindjiliya et al. [18] during the machining of titanium alloys, with the greatest influence on the fatigue behavior in the range of VB = 0.05 mm to VB = 0.25 mm.

As a result of mechanical and thermal loads from the machining process, internal material loads such as stresses, strains, temperatures, etc. occur. This induces material changes on the surface and in the bulk, e.g., changes in hardness, residual stresses or phase transformations. Functional properties such as wear resistance or fatigue strength are influenced, too [19]. Tool engagement causes plastic deformation of the material surface and the edge zone, mainly due to shear deformation and friction between the tool flank and the workpiece material. Such mechanical loads often lead to residual compressive stresses.

Lai, Huang and Buising [20] experimentally investigated the effects of surface roughness on the fatigue strength of hardened (bainitic and martensitic) steel and a tough tempered medium carbon steel 50CrMo4 (SEA 4150H). Since the percentage of crack initiation in the overall lifetime of specimens generally increases with increased brittle behavior, surface roughness has a greater impact on hardened steel than on normalized steel. In case of lower stress amplitudes and therefore higher numbers of cycles to failure the damage process changes. Especially inclusions and pores are starting points for crack initiation considering a Very-High-Cycle-Fatigue (VHCF) loading. As a result, the influence of the surface conditions becomes less important. For rough surfaces, the failure mode tends to be dominated by surface fatigue. Fracture of the unhardened steel is primarily caused by surface cracks. That's why the fatigue strength decreases with increasing surface roughness. Lai, Huang and Buising [20] also developed a unified model for predicting the S-N property, taking the effects of surface roughness and the defect susceptibility of the material structure into account.

The machining process is characterized by a short-term increase in temperature in the cutting zone and high thermal loads. Self-quenching and quenching by the cooling lubricant lead to a rapid cooling of the temperature-affected area. As a result of thermal loads, tensile or compressive residual stresses depending on the workpiece material can occur [21,22]. To take the effects of macroscopic geometric discontinuities on the strength of components into account, usually the stress concentration factor Kt is used. Here, Kt only depends on the notch shape (notch height and notch root radius) [23,24]. According to the semi-empirical Neuber relationship for the surface stress concentration factor, it is complemented by standard roughness parameters and stress state [23,25]. The effective elastic stress concentration Kt,e for the process-dependent surface texture is expressed by standard roughness parameters in combination with the effective profile valley radius and the stress state [23,26].

Materials and Methods

Material. The investigated material is a low-alloyed 1.6310 steel (20MnMoNi5- 5), mainly used as a spray line material in German nuclear power plants. Micrographs, taken with a digital microscope, as well as with a scanning electron microscope are given in Figure 1. The ferritic-bainitic microstructure evidently exhibits a large number of carbides, especially along grain boundaries. A more detailed analysis of the investigated material is given in Table 1.

Table 1: Chemical composition of the investigated 1.6310 steel (according to own analysis)

Element	C	Si	Mn	Cr	Ni	Mo	S	P
wt.%	0.218	0.246	1.385	0.076	0.762	0.487	0.003	0.01

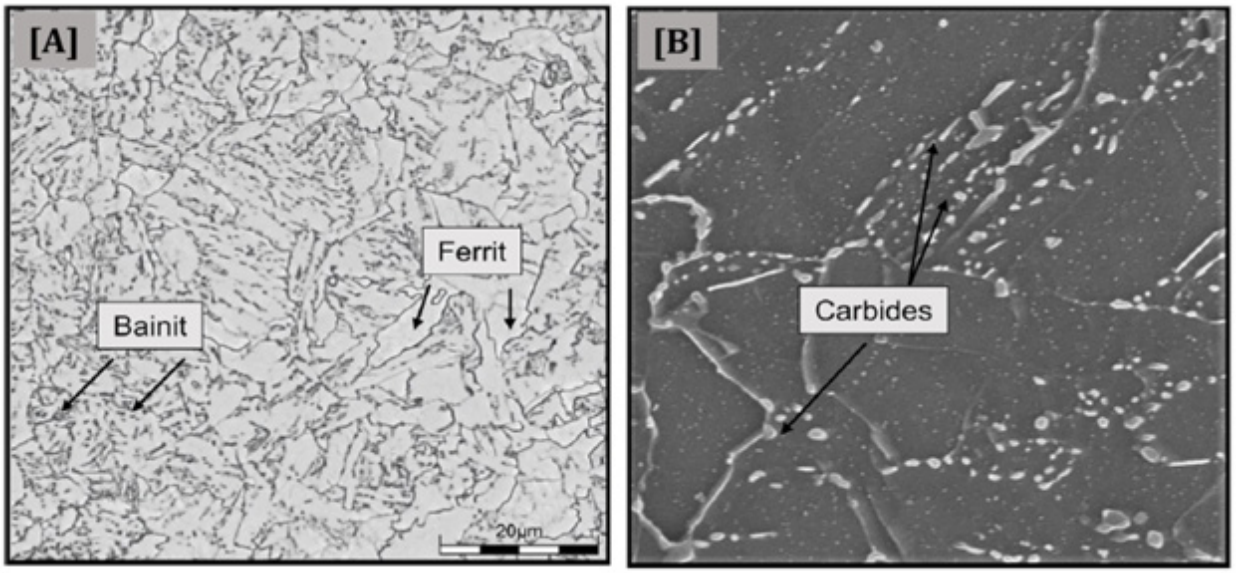

Figure1: Micrographs using digital (EVIDENT DSX 1000) [A] and scanning electron microscopy (ZEISS Gemini) [B]

Specimen manufacturing. The specimens were separated from pipes with an inside diameter of 706 mm and a thickness of 47 mm. For the heat-treatment of the pipes, the austenitization was carried out at a temperature of 910°C, followed by water quenching and tempering at a temperature of 680°C for 40 min.

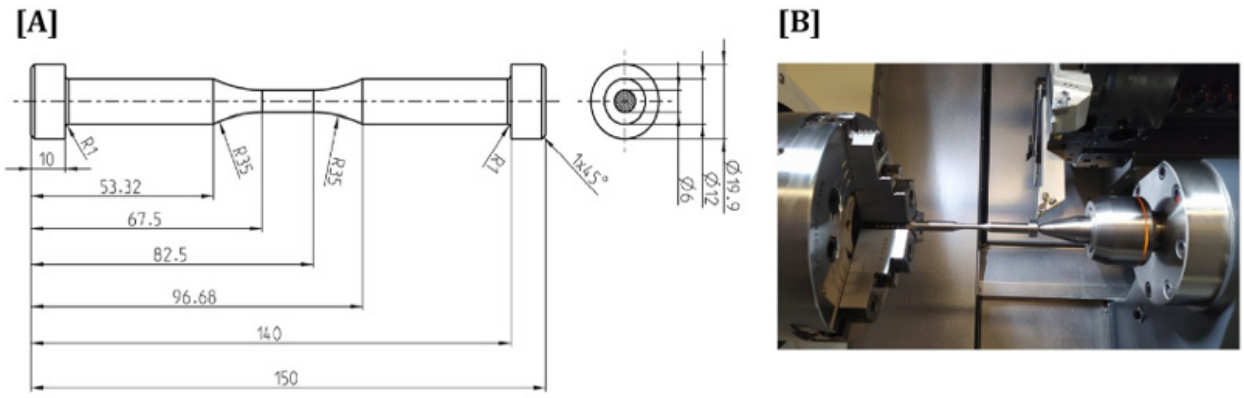

Figure2: Dimension of the specimens [A] and specimen manufacturing in the lathe [B]

Manufacturing of specimens is done on a computer numerical controlled (CNC) lathe type DMU T2 (see Figure 2 B), where the cooling is realized through an 8 % oil-water emulsion type KLUTE Hakuform A846BF. The coolant supply is carried out as an external overflow cooling with a pressure of 8 bar. The clamping in the lathe was realized in a three-jaw chuck and a tailstock with a contact pressure of 8.6 bar.

The total specimen length is set to 150 mm. At both ends of the specimens was a cylinder of 10 mm length and 19.9 mm diameter for clamping the specimen in the fixture of the testing machine (see Figure 2 A). The distance between the shoulders is 130 mm, with two cylindrical sections of 12 mm diameter, whereas the constriction is characterized by a diameter of 6 mm.

The roughing toolpath used for turning the cylindrical part started 2 mm from the clamping end and had a 15 mm radius to allow the lathe spindle to reach the required revolutions before the insert cutting tool contacted the surface for the first time. The basic contour of the specimen was generated by four roughing oper-ations. The parameters for the roughing process are cutting speed vc = 100 m × min^{-1}, feed rate f = 0.3 mm × rev^{-1}, and depth of cut a_p = 1.3 mm.

The finishing toolpath used for creating the constriction starts at a radius of 35 mm. The cutting parameters for the finishing operations are shown in Table 2. Batches B, C and D are each treated with identical machining parameters with increasing tool wear (increasing width of flank wear VB and cutting edge rounding rB). Batch A, like Batch B, is manufactured with new tools without wear. In batch A, a reduced feed rate was chosen, and a polishing process was carried out after the turning process. This further reduces the surface roughness and induces residual compressive stresses in the surface area of the workpiece. The specimens produced in this way serve as a reference in terms of their surface integrity.

Table 2: Cutting Parameters and tool wear condition.

Batch	Feed Rate [mm x rev^{-1}]	Cutting Speed [m x min^{-1}]	Depth of Cut [mm]	Tool Wear (see Figure 5)
A (Comparison group)	0.05	12	0.2	[0]
B	0.2	12	0.2	[0]
C	0.2	12	0.2	[I]
D	0.2	12	0.2	[II]

Cutting tools. For the roughing operations, carbide inserts from type HOLEX DCMT11T308-MM with 0.8 mm tool tip radius (r_ε), positive rake angle and TiCN coating are used. The insert has a chip breaker type MM to reduce the occurrence of work -hardened chips and thus homogenize the surface quality of the machined workpieces by reducing surface notches. For every manufactured specimen batch, a new insert was used.

For the finishing operation, carbide inserts from type GARANT DCMT 11T308 with 0.8 mm tool tip radius are used. The insert has a chip breaker from type SS and a simple TiN coating, which allows a comprehensive view for the tool wear. For every manufactured specimen batch, an insert with a defined state of wear was used. These defined worn inserts were produced by using them in an external cylindrical machining process of 1.7218 (500 HV). Thus, the wear behavior of new inserts and their wear progression curve could be determined. In order to specifically wear the tools, this material was chosen because experience has shown that reproducible wear phenomena occur with appropriate cutting paths. The specimens were machined with new inserts on a WEILER 160 CNC lathe from a diameter of 30 mm to a diameter of 6 mm. They were clamped in the lathe with a three-jaw chuck and a tailstock. The cooling was realized with an 5 % oil-water emulsion type HENKEL Multan 71-10 SK.The cutting parameters were a_p = 0.8 mm, v_c = 200 m x min^{-1} und f = 0.2 mm x rev^{-1}. After each sample machined in this way, the wear condition of the insert was determined. For this purpose, a LEICA DMS 1000 measuring microscope was used to determine the width of the flank wear. The cutting edge rounding was measured using a ZEISS SmartProof 5 confocal microscope.

For the surface polishing of the specimens from batch A, a grinding and polishing paste with an equivalent particle size of 6,000 and 12,000, respectively, as well as a polishing felt by ROTWEISS24, was used.

Surface Roughness. A ZEISS Smartproof 5 confocal microscope and an EVIDENT LEXT OLS5100 laser scanning microscope are used to measure the surface roughness profile and various roughness parameters such as R_a and R_z. Figure 3 shows a schematic representation of where the surface roughness is determined by using the confocal microscope. To ensure a statistically reliable evaluation of the sample roughness, each sample is measured at a total of 12 measuring points (3 measuring points every 90°, in the middle of the gauge length and before the transition to the radius) [27]. Surface roughness profiles with the laser scanning microscope were created by means of axial measuring sections with a length of 1,250 µm in the center of the constriction.

Fatigue testing. Fatigue tests were carried out under stress-controlled conditions at room temperature with a load ratio of R=-1 using a sinusoidal load-time function on a 20 kN servo-hydraulic testing rig (type EHF-L from the company Shimadzu). The load frequency was 5 Hz. Figure 4shows the complete test setupof the 20 kN testing rig. The use of different measurement methods makes it possible to obtain as much information as possible about the fatigue processes in the various stages of the specimen's lifespan. For this purpose, the measurement setup includes thermographic, electrical, optical and tactile methods for data acquisition.

Results and Discussion

Tool wear progress. Figure 5 (A) shows the development of the wear progress with increasing cutting path l_c of the finishing tools used in this work. The development of the main cutting edge rounding r_B (red) and the width of flank wear VB on the main tool flank face (blue) show the form of typical wear progress curves. After a degressive start, both curves are characterized by a pronounced quasi-stationary range. From a cutting path of $l_c \approx$ 28,000 m, breakouts evidently occur on the tool's cutting edges and the progress of the wear variables under consideration changes to a progressive curve. At a cutting path of $l_c \approx$ 32,000 m, the end of the tool life is

reached due to large cutting edge chipping. The following typical tool wear conditions were selected for the further investigations (Figure 5 B): [0] l_c = 0 m (new tool), [I] l_c = 20,000 m (steady-state wear range) and [II] l_c= 30,000 m (severe wear shortly before end of tool life).

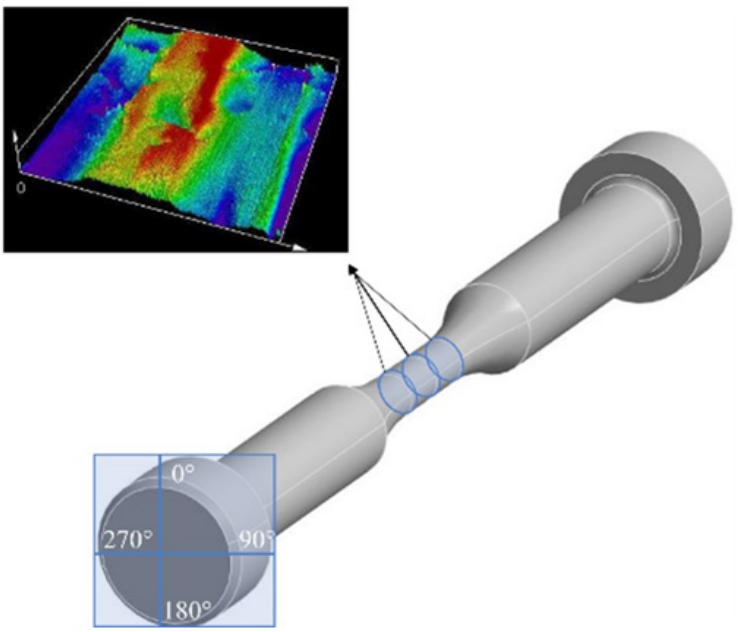

Figure 3: Positions for determining the surface roughness parameters.

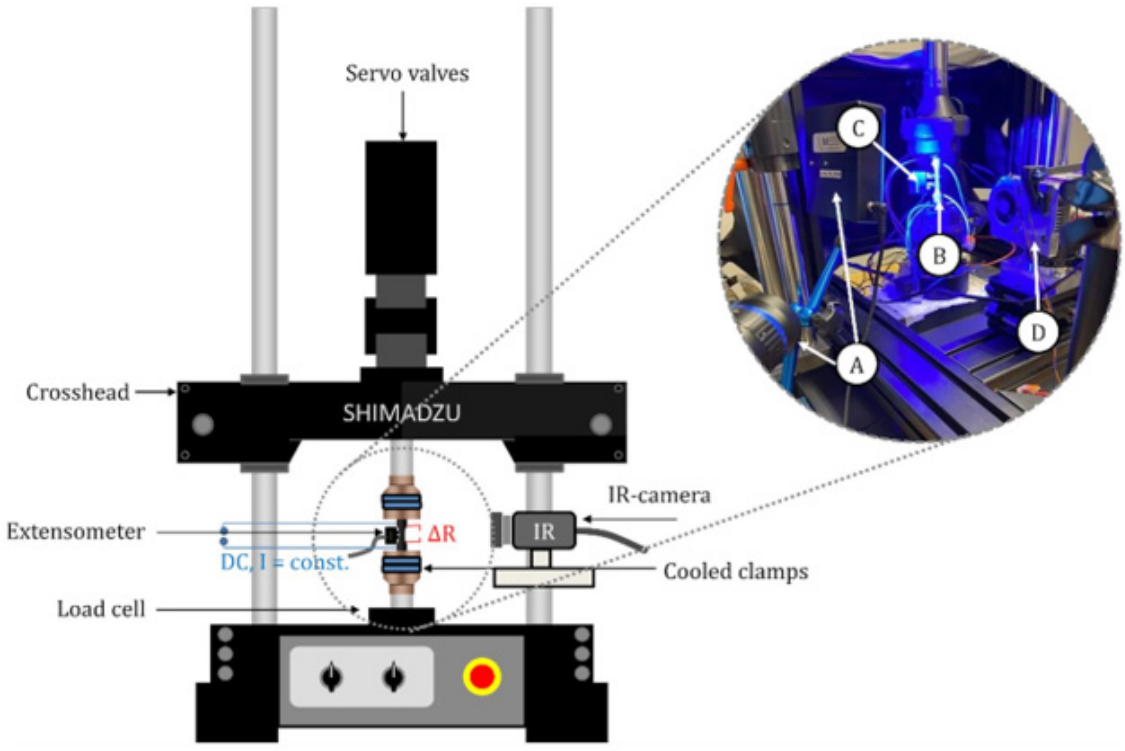

Figure 4: Schematic illustration of the servo hydraulic testing rig (left) and applied measurement technology (right): (A) Digital Image Correlation (Camera and illumination unit); (B) Electrical resistance Measurement; (C) Tactile extensometer; (D) IR-camera.

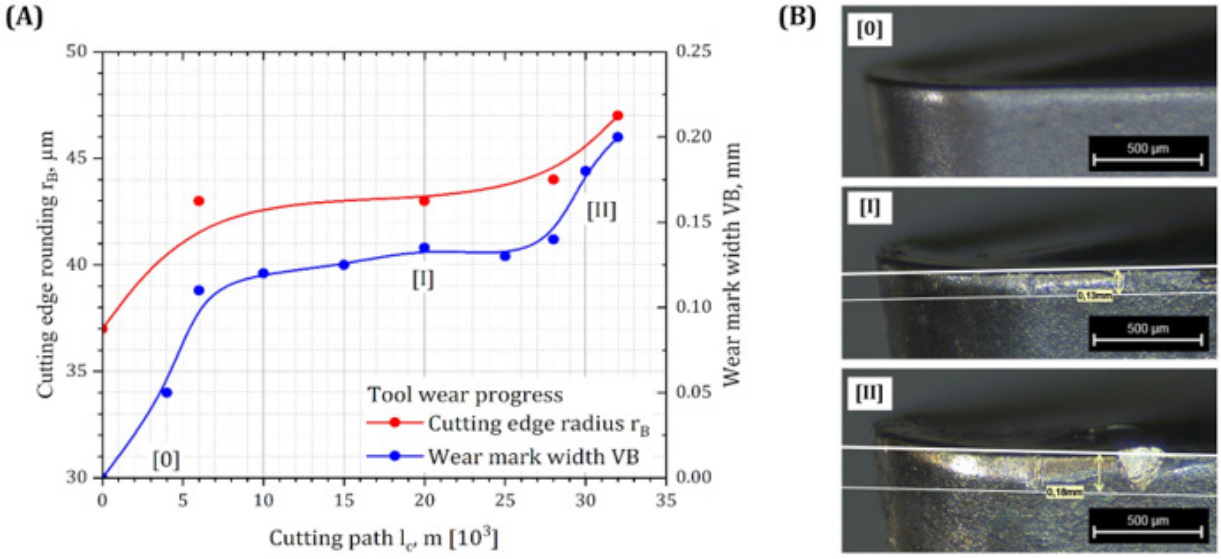

Figure 5: Wear progress of the finishing tools (A) and selected wear conditions for the further investigations (B).

Figure 6 shows the measured roughness height of the specimens over the axial measuring section in the center of the constriction. The green curve shows the roughness height for specimens machined with unworn new tools (TW0, Batch B). The peaks in the curve have a distance of ΔGL ≈ 200 µm and thus correspond to the machining feed rate of f = 0.2 mm × rev^{-1}, as expected. The maximum difference in roughness height ΔR is ≈ 6.8 µm and thus corresponds to the expected the maximum roughness height according to [28]:

$$R_{max(real)} = 1.14 \times R_{max} + 0.3 \qquad (1)$$

The determined value for $R_{max(real)}$ is a function of the theoretical parameter R_{max}, which is defined in

$$R_{max} = \frac{f^2}{8 \times r_\varepsilon} \qquad (2)$$

At this point it should be noted that the relation according to equation (1) is based on the results of a 34CrNiMo6 (SAE 4340). Nevertheless, there is still a comparability due to the fact that in both cases it is a low alloyed-steel with similar alloying elements. The blue curve shows the roughness height for specimens in the reference group (Batch A), which were machined with unworn new tools (TW0) and additionally polished after the turning process. As a result, the cutting edge engagement of the turning tool is no longer recognizable.

Batch C (golden gradient) and Batch D (red gradient) were produced with tools that were worn to varying degrees (TWI and TWII). Due to the increased width of flank wear VB and cutting edge rounding r_B, the contact surface of the tool to the workpiece is increased during the cutting process. This leads to increased vibration in the machining process, which results in the surface waviness with simultaneously increasing roughness that can be seen in the curves.

As expected, increasing tool wear leads to an increase in the roughness parameters R_a and R_z. Based on the measured R_a, the manufactured batches can be assigned to the roughness indicators N5 - N9 according to DIN EN ISO 1302 [29], representing the corresponding specimen surface conditions.

In Figure 7, the results of the investigation are shown in mutual dependence. The number of cycles to failure N_f of the fatigue test are shown as a function of the stress amplitude σ_a and the surface condition N_i. The specimens were tested at the three different load levels in order to cover a wide range of the HCF-regime. The selected stress amplitude of σ_a = 360 MPa leads to fatigue failure near the transition to the VHCF regime, whereas a dynamic loading with σ_a = 400 MPa results in data points in the transition to the LCF - (Low-Cycle -Fatigue) regime. The colors of the data points indicate the respective tool wear condition. The blue points, serving as a reference, indicate specimens which were produced with new tools without wear but with reduced feed rate. In order to achieve the highest surface quality, these components were mechanically polished after the turning process, which on the one hand further reduced the surface roughness. On the other hand, the polishing process also induced residual compressive stresses in the component edge zones. Against this background, the blue points are only comparable with the green points due to the same tool wear condition.

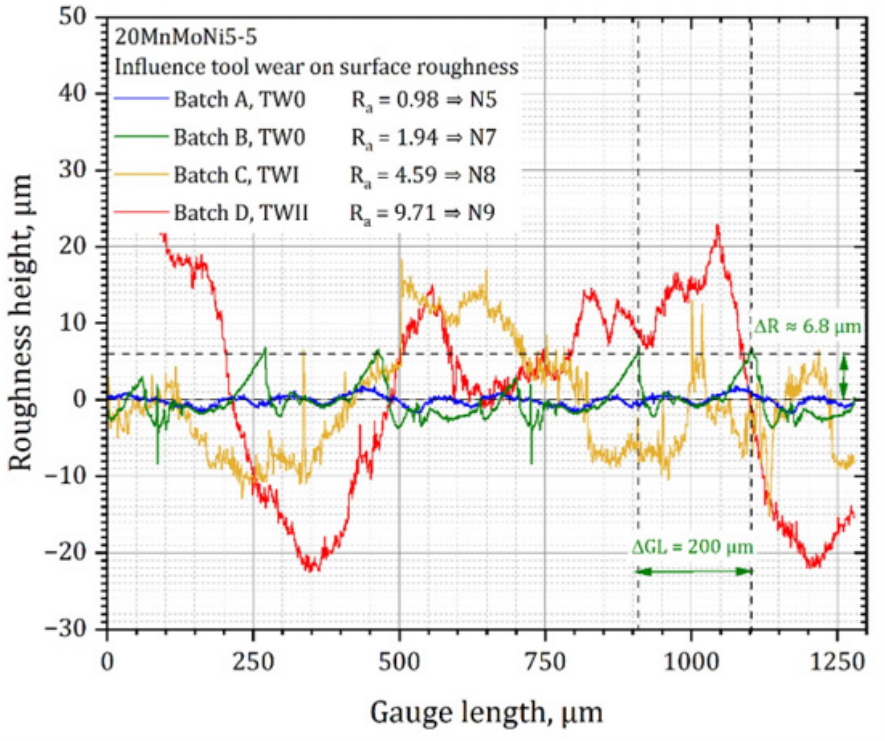

Figure 6: Influence of tool wear (TW0-TWII) on surface roughness of the specimens.

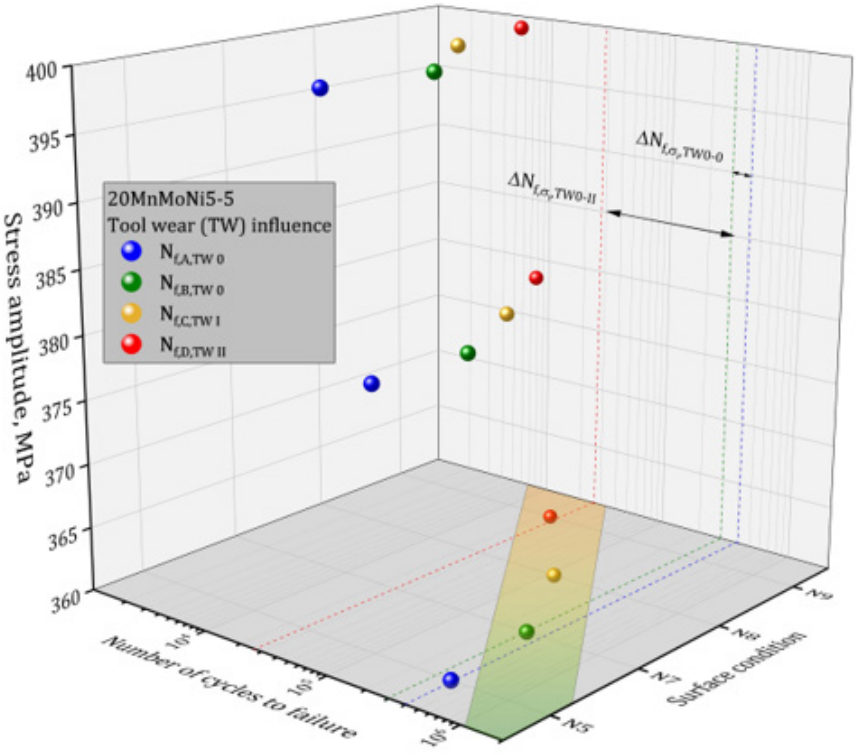

Figure 7: Correlation of tool wear condition, surface conditions, stress amplitude and fatigue lifetime of a 1.6310 steel.

A comparison of the numbers of cycles to failure of the different surface conditions (N7-N9) leads to the insight that an increased surface roughness results in a decreasing lifetime of the specimens. Because of the polishing process, which leads to increased compressive residual stresses, the reference batch N5 is deliberately excluded at this point. The percentage lifetime reduction for each stress amplitude is given in Table 3. The reason for the reduced lifetime with increasing surface roughness is that roughness grooves act as some kind of multi-notch. These areas with locally increased stress concentrations are starting points for microcracks. Especially in case of more brittle material behavior, which includes the investigated 1.6310 steel, most of the fatigue life is determined by crack initiation. Therefore, if the aspect of crack initiation is facilitated by surface factors, a significant lifetime reduction can be expected.

Table 3: Change in the number of cycles to failure for different stress amplitudes depending on the tool wear condition and the surface roughness

Stress amplitude σ_a [MPa]	$\Delta N_{f,\sigma_a,TW0-II}$ [%]	$\Delta N_{f,\sigma_a,TW0-0}$ [%]
400	-78.9	34
380	-83.9	4.8
360	-92.3	-21.6

With $\Delta N_{f,\sigma a,TW}$ a percentage change in the number of cycles to failure can be specified as a function of the stress level σ_a and the tool wear conditions (TW) on which the specimen surface conditions are based (see Table 3)

With $\Delta N_{f,\sigma a,TW0-II}$, this change is shown in comparison with an unworn new tool (TW0) and a severely worn tool shortly before the end of its service life (TWII). As the stress amplitude increases, $\Delta N_{f,\sigma a,TW0-II}$ decreases significantly, resulting from different damage mechanism in the LCF-regime compared to the HCF-regime. This reduces the influence of the surface roughness caused by the tool wear condition on the fatigue strength of the specimen.

$\Delta N_{f,\sigma a,TW0-0}$ shows the percentage change in the number of cycles to failure for a new tool (TW0) versus the reference group. Both batches were machined using the same machining parameters with the exception of the mechanical polishing process in case of the N5 batch. Compressive residual stresses in general, result in an increased lifetime as occurring microcracks are prevented from further propagating. However, the influence of residual stresses also depends on the stress amplitude, which can be seen in Table 3. In case of lower load levels, residual stresses partially exceed the applied load amplitude and therefore lead to an increase in the fatigue life, which is also reflected in Table 3. As the external stress amplitude increases, the influence decreases significantly, since residual stresses can be reduced rapidly. Since an extension of the fatigue lifetime of the N7 specimens compared to the N5 batch in case of high stress amplitudes is not physically meaningful, the positive values in Table 3 can be explained by material-related scattering of the fatigue life.

Conclusion

The objective of the present work was to evaluate the influence of tool wear on the fatigue strength for the ferritic-bainitic steel 1.6310 (20MnMoNi5-5). Therefore, the relationship between the wear condition of the turning tools, represented by flank wear and cutting edge rounding, and the surface roughness of machined specimens and their influence on fatigue strength is presented.

The key findings of the presented research can be summarized in the following way:

- The characteristics of surface roughness meet the expectations, that increasing tool wear leads to an increase in the roughness parameters R_a and R_z. The peaks in the roughness height correspond to the machining feed rate and the maximum difference in roughness height to the expected maximum roughness height.
- As expected, the results show a reduction in the number of cycles to failure as the stress level σ_a increases. Regardless of the stress level, a correlation between the surface condition classes and the number of cycles to failure can be seen.
- In summary, it can be stated that with increasing stress amplitude σ_a, both the influence of the tool wear condition and the influence of the surface integrity vary. Depending on the stress level, it may therefore be possible to manufacture components with progressively worn tools (larger VB and r_B) in terms of fatigue strength.

Acknowledgement

This research is supported by the German Federal Ministry for the Environment, Nature Conservation, Nuclear Safety and Consumer Protection (BMUV, grant number: 1501623). Furthermore, the authors would like to thank the project management agency GRS (Gesellschaft für Anlagen-, und Reaktorsicherheit), the University of Applied Sciences Kaiserslautern for financial support in the procurement of test infrastructure, Shimadzu Europe and EVIDENT (former Olympus) for their support in technical equipment provision. The authors would also like to thank Prof. Dr.-Ing. habil. Peter Starke, who also contributed to the development of the presented research results through his consulting work.

Conflict of Interest

The authors declare no conflicts of interest.

References

1. V Gvindjiliya, E Fominov, D Moiseev, T Lavrenova (2024) Evaluation of tribo-vibration characteristics of the finishing turning process of heat-resistant structural steel 20MnMoNi5-5. E3S Web Conference (Tashkent) 515: 02012.
2. F Weber, R Acosta, T Eyrisch, T Hielscher, M Magin, P Starke, et al. (2019) Influence of processing parameters on the fatigue life time of specimens made from quenched and tempered steel SAE 4140H. Materials Testing 61(9): 842-850.
3. F Zhujani, G Todorov, K Kamberov, F Abdullahu (2023) Mathematical Modeling and Optimization of Machining Parameters in CNC Turning Process of Inconel 718 using the Taguchi Method. Journal of Engineering Research.
4. A Şencan, Ş Şirin, E Saraç, B Erdoğan, M Koçak (2024) Evaluation of machining characteristics of SiO_2 doped vegetable based nanofluids with Taguchi approach in turning of AISI 304 steel. Tribology International 191: 109122.
5. S Prashantha Kumar, H Thirthaprasada, M Nagamadhu (2020) Multi-Response Optimization of Parameters in Turning of DSS-2205 using Hybrid (Al_2O_3+CuO) Nano Cutting Fluid with MQL. Tribology in Industry 42(4): 641-657.
6. A Ebrahimi, M Moshksar (2009) Evaluation of machinability in turning of microalloyed and quenched-tempered steels: Tool wear, statistical analysis, chip morphology. Journal of Materials Processing Technology 209(2): 910-921.
7. T Childs, K Maekawa, T Obikawa, Y Yaman (2000) Metal Machining: Theory and Applications. Arnold, London.
8. E Trent, P Wright (2000) Metal Cutting. Butterworth-Heinemann, Boston.
9. J Wang, CZ Huang, WG Song (2003) The effect of tool flank wear on the orthogonal cutting process and its practical implications. Journal of Materials Processing Technology 142(2): 338-346.
10. S Choudhury, K Kishore (2000) Tool wear measurement in turning using force ratio. International Journal of Machine Tools and Manufacture 40(69): 899-909.
11. A de Farias, SLR de Almeida, S Delijaicov, V Seriacopi, E C Bordinassi, et al. (2020) Simple machine learning allied with data-driven methods for monitoring tool wear in machining processes. International Journal of Advanced Manufacturing Technology 109: 2491-2501.
12. P Varela, C Rakurty, A Balaji (2013) Surface integrity in hard machining of 300M steel: Effect of cutting-edge geometry on machining induced residual stresses. Procedia CIRP 13: 288-293.
13. A Reimer, X Luo (2018) Prediction of residual stress in precision milling of AISI H13 steel. Procedia CIRP 71: 329-334.
14. A Reimer, X Luo (2018) Prediction of residual stress in precision milling of AISI H13 steel, Precidia CIRP 71: 329-334.
15. I Jawahir, E Brinksmeier, R Saoubi, D Aspinwall, J Outeiro, et al. (2011) Surface integrity in material removal processes: Recent advances. CIRP Annals - Manufacturing Technology 60: 603-626.
16. M Liu, J Takagi, A Tsukuda (2004) Effect of tool nose radius and tool wear on residual stress distribution in hard turning of bearing steel. Journal of Material Processing Technology 150(3): 234-241.
17. Z Fangyuan, D Chunzheng, S Wei, J Kang (2019) Effects of cutting conditions on the microstructure and residual stress of white and dark layers in cutting hardened steel. Journal of Material Processing Technology 266: 599-611.
18. L Xun, W Ziming, Y Shenliang, G Zhiyuan, Z Yongxin, et al. (2021) Influence of turning tool wear on the surface integrity and anti-fatigue behavior of Ti1023. Advances in Mechanical Engineering 13(4).
19. E Brinksmeier, D Meyer, C Heinzel, T Lubben, J Solter, et al. (2018) Process Signatures – The Missing Link to Predict Surface Integrity in Machining. Procedia CIRP 71: 3-10.
20. J Lai, H Huang, W Buising (2016) Effects of microstructure and surface roughness on the fatigue strength of high-strength steels. Procedia Structural Integrity 2: 1213-1220.
21. B Denkena, H Tönshoff (2011) Machining – the Basics (Spanen – Grundlagen), 3rd Ed. Springer-Verlag, Heidelberg.
22. F Klocke (2018) Manufacturing Processes 1 – Machining with geometrically defined cutting edges (Fertigungsverfahren 1 – Zerspanung mit geometrisch bestimmter Schneide), 9th Ed. Springer, Berlin.
23. D Arola, C Williams (2002) Estimating the fatigue stress concentration factor of machined surfaces. International Journal of Fatigue 24(9): 923-930.
24. R Peterson (1974) Stress Concentration Factors, John Wiley and Sons, New York.
25. H Neuber (1958) Notch stress theory (Kerbspannungslehre). Springer, Berlin.
26. D Arola, M Ramulu (1999) An examination of the effects from surface texture on the strength of fiber-reinforced plastics. Journal of Composite Materials 33(2): 101-86.
27. F Weber, P Starke (2024) Implementation of modelled surface roughness in the accelerated lifetime prediction of a 20MnMoNi5-5 steel. International Journal of Fatigue 186: 108391.
28. A Javidi, U Rieger, W Eichlseder (2007) The effect of machining on the surface integrity and fatigue life. International Journal of Fatigue 30(10-11): 2050-2055.
29. B V GmbH (2002) Geometrical Product Specifications (GPS) – Indication of surface texture in technical product documentation (ISO 1302:2002), Beuth Verlag GmbH p. 1.